Applied Catalysis B: Environmental 154–155 (2014) 213–220

Contents lists available at ScienceDirect

Applied Catalysis B: Environmental

journal homepage: www.elsevier.com/locate/apcatb

Ni_3S_2/carbon nanotube nanocomposite as electrode material for hydrogen evolution reaction in alkaline electrolyte and enzyme-free glucose detection

Tsung-Wu Lin[a,b,*], Chia-Jui Liu[a,b], Chao-Shuan Dai[a,b]

[a] Department of Chemistry, Tunghai University, No. 181, Sec. 3, Taichung Port Road, Taichung City 40704, Taiwan
[b] Tunghai Green Energy Development and Management Institute (TGEI), Tunghai University, No. 181, Sec. 3, Taichung Port Road, Taichung City 40704, Taiwan

ARTICLE INFO

Article history:
Received 2 September 2013
Received in revised form 30 January 2014
Accepted 11 February 2014
Available online 20 February 2014

Keywords:
Nickel sulfide
Carbon nanotubes
Nanocomposite
Electrocatalyst
Hydrogen evolution

ABSTRACT

In this study, the nanocomposite of Ni_3S_2 and multi-walled carbon nanotubes (MWCNTs) with the high catalytic activities toward hydrogen evolution reaction (HER) and glucose oxidation was synthesized using glucose-assisted hydrothermal method. Ni_3S_2 nanoparticles with the diameters ranging from 10 to 80 nm were highly dispersed over conductive MWCNT surface. A series of linear polarization measurements suggested that the HER activity of nanocomposite of Ni_3S_2 and MWCNTs was increased with decreasing the loading amount of Ni_3S_2 on MWCNTs and the optimal Ni_3S_2 loading on MWCNTs was 55 wt%. Furthermore, the immersion of the composite catalyst in a concentrated KOH solution induced the morphological change of the Ni_3S_2 nanoparticles on MWCNTs, which increases the active surface area of the composite electrode. As a result, the KOH-treated composite electrode showed a higher HER activity than other electrodes. For example, the value of exchange current density of the KOH-treated composite electrode was ca. 395 times and 1.6 times larger than that of Ni_3S_2 electrode and as-synthesized composite, respectively. Furthermore, the impedance measurements showed the KOH-treated composite electrode had the smaller charge transfer resistance of the HER than Ni_3S_2 electrode. Based on the slopes obtained from Arrhenius curves of the electrodes, the estimated HER activation energy (71.8 kJ/mol) of KOH-treated composite electrode was only one-third of that of the pure Ni_3S_2 electrode. The high catalytic activity of the KOH-treated composite electrode was stemmed from the synergistic effect of the large active surface area of Ni_3S_2 nanoparticles and the excellent electrical coupling to the conductive MWCNT network. More importantly, the current density of KOH-treated composite electrode showed no sign of degradation after the continuous 1000 cycling in a 1 M KOH solution at the temperature of 323 K. On the other hand, the nanocomposite of Ni_3S_2 and MWCNTs was proposed for the first time as an enzyme-free sensor for glucose. The Ni_3S_2 nanoparticles on MWCNTs exhibited high electrocatalytic activity toward glucose oxidation and were insensitive to uric acid and ascorbic acid. Furthermore, the composite electrode exhibited that its catalytic current was linearly dependent on the concentration of glucose in the range from 30 to 500 μM and its sensitivity was as high as 3345 μA/mM. The present work suggested that the nanocomposite of Ni_3S_2 and MWCNTs not only served as an inexpensive, highly active and stable electrode material for alkaline water electrolysis, but also showed a great potential application as a highly sensitive and selective biosensor for glucose.

1. Introduction

The demand for environmentally friendly energy resources gradually becomes urgent and important due to climate change and the limited availability of fossil fuels. In the recent years, hydrogen has been viewed as the clean and efficient fuel source that can be used in the vehicles and fuel cells [1,2]. Conventionally, large scale production of hydrogen can be achieved by natural gas reforming, and gasification of coal and petroleum coke [3,4]. The main drawbacks of the aforementioned methods include the use of non-renewable energy source, the release of carbon dioxide and high reaction temperature. As a result, a lot of efforts have been devoted to producing hydrogen from water splitting through either electrochemical process or photocatalytic route [5–7]. Compared

* Corresponding author at: Department of Chemistry, Tunghai University, No. 181, Sec. 3, Taichung Port Road, Taichung City 40704, Taiwan.
Tel.: +886 4 23590121x32250.
E-mail address: twlin@thu.edu.tw (T.-W. Lin).

http://dx.doi.org/10.1016/j.apcatb.2014.02.017
0926-3373/

with photocatalytic water splitting, water electrolysis is an easier method to produce hydrogen. Due to the fact that most of electrode materials suffer from corrosion in acid, alkaline water electrolysis is widely adopted in industry. Besides platinum, nickel is the most important and widely studied electrode material for alkaline water electrolysis due to its high activity toward hydrogen evolution reaction (HER), availability and low cost [8]. However, nickel cathode undergoes significant deactivation during alkaline water electrolysis [9–11]. Among the promising alternative cathode materials, the Ni-based materials including Ni–Mo, Ni–W, Ni–Co, and Ni–Zn alloys have attracted considerable attention due to their high HER activity and corrosion resistance in alkaline media [12–15]. Compared with other binary Ni alloys, Ni–S alloy has been recognized as a superior electrocatalyst for the alkaline electrolysis due to its easy preparation and low cost [16–20]. The previous studies have suggested that the HER activities of Ni–S alloy electrodes are closely relevant to sulfur contents in alloys, the crystallinity of the Ni–S alloy, and the active surface area of electrode material [18–20]. In principle, the activity of HER catalysts can be improved by increasing the real surface area and/or the intrinsic activity of the catalysts. The increase in the real surface area of the electrocatalyst can be achieved by dispersing it onto the carbon materials with high surface area. Such method has been well demonstrated by the recent studies where nanoscale catalysts for HER are homogeneously dispersed over the conductive carbon nanomaterials (CNs) such as graphene and multi-walled carbon nanotubes (MWCNTs) [21–24]. The combination of CNs with the HER catalyst should provide some additional advantages. For example, the high conductivity of CNs allows the electrons to be easily shuttled to the catalyst. Furthermore, the great chemical and mechanical stability of CNs should improve the stability of the catalyst in the long-term operation.

To the best of our knowledge, the effect of combining conductive carbon nanomaterial with Ni–S compound on the HER activity of the catalyst has not been studied systematically. In this work, the nanocomposite of Ni_3S_2 and MWCNTs (Ni_3S_2/MWCNT-NC) is synthesized using glucose-assisted hydrothermal method and its HER activity and kinetics are investigated. To understand the origin of the HER activity of Ni_3S_2/MWCNT-NC, the role of MWCNTs in the catalyst and the effect of catalyst's morphology are discussed. It is demonstrated that Ni_3S_2/MWCNT-NC exhibits the superior HER activity to pure Ni_3S_2 electrode due to the fact that the former has the relatively small HER activation energy (E_a). Furthermore, Ni_3S_2/MWCNT-NC shows the reasonable stability in the long-term operation. On the other hand, the Ni_3S_2/MWCNT-NC electrode is proposed for the first time as an enzyme-free sensor for glucose. It is found that the Ni_3S_2 nanoparticles deposited on MWCNTs exhibit high electrocatalytic activity toward glucose oxidation. The performance of glucose sensor based on Ni_3S_2/MWCNT-NC is examined by cyclic voltammetry (CV) and amperometric methods, which shows a good linear dependence on glucose concentration, and high sensitivity and selectivity to glucose.

2. Experimental

2.1. Synthesis of Ni_3S_2/MWCNT-NC

The purification of MWCNTs was achieved by refluxing MWCNTs (0.5 g) in concentrated nitric acid (100 ml) at 120 °C for 12 h. After the reaction, the MWCNT precipitate was filtered off, washed with distilled water and dried in air. For the synthesis of Ni_3S_2/MWCNT-NC, acid-treated MWCNTs (7.5 mg) and glucose (90 mg) were added to the mixture solution of ethanol (9 ml) and distilled water (1 ml). The mixed solution was sonciated for 20 min to make a homogeneous dispersion and then nickel chloride, thiourea and 1 ml of ammonia were added to the MWCNT dispersion. For the synthesis of the composites with 38, 49, 55, 70 and 83 wt% Ni_3S_2, 3.05, 6.1, 12.2, 24.3 and 48.6 mg of nickel chloride and 1.2, 2.4, 4.8, 9.5 and 19 mg of thiourea were used, respectively. The mixture was then transferred to a stainless-steel autoclave (20 ml capacity). After sealing, the autoclave was heated to 180 °C for 12 h and then cooled to room temperature. Finally, the precipitate was filtered off, washed with distilled water and dried in air. The loading amount of Ni_3S_2 in the composite can be approximated by the following equation.

$$Ni_3S_2\ \text{wt\% in the composite} = \frac{M_c - M_m}{M_c} \times 100\%$$

where M_c and M_m are the mass of as-synthesized composite and MWCNTs, respectively.

2.2. Material characterizations

Field-emission transmission electron microscope (TEM, JEOL JEM-2100F, operated at 200 kV with a point-to-point resolution of 0.19 nm) equipped with an energy dispersive spectrometer (EDS) was used to obtain the information on the microstructures and the chemical compositions. X-ray powder diffraction (XRD) pattern of the composite was obtained from Philips X'Pert Pro MPD.

2.3. HER characterizations of Ni_3S_2/MWCNT-NC

In the study of the HER activity of the nanocomposite, 1 mg of catalyst and 80 μl of 5 wt% Nafion solution were mixed in 10 ml of ethanol and the mixed solution was sonicated for 10 min to form a homogeneous ink. Then the catalyst of 50 μg was drop-cast onto a silver electrode of 5 mm in diameter, which serves as a working electrode. Linear sweep voltammetry (Autolab PGSTAT-128 N) with scan rate of 1 mV/s was conducted in a 1 M KOH solution using Ag/AgCl (sat. KCl) electrode as the reference electrode and a Pt wire as the counter electrode. The electrochemical impedance spectroscopy (EIS) measurements were performed in the same configuration at the overpotential (η) of 0.4 V from 10^6 to 0.02 Hz with an AC voltage of 5 mV. The complex nonlinear least square (CNLS) analyses of the resulting EIS spectra were conducted using the software ZSimpWin version 3.1. The standard error after the best-fit values for each equivalent circuit parameter is less than 5% when using the proposed equivalent circuit model in this study.

2.4. Glucose detection

The sensors were prepared by mixing Ni_3S_2/MWCNT-NC with carbon black and polyvinylidene difluoride at a weight ratio of 8:1:1. After thorough mixing, the slurry was pressed onto Ni foam (10 mm × 10 mm × 1 mm) and then dried at 60 °C in vacuum for 1 day. The loading of slurry on the Ni foam was approximately 0.6 mg. All electrochemical measurements were performed in a standard three-electrode cell. CV and amperometric measurements were performed using a CHI 635A electrochemical workstation.

3. Results and discussion

3.1. Structural and compositional characterizations of Ni_3S_2/MWCNT-NC

Fig. 1a–c shows the typical TEM images of the MWCNTs loaded with the various amount of Ni_3S_2 nanoparticles. It is clear to see that conductive MWCNTs can serve as the backbone where the nanoparticles with the diameters ranging from 10 to 80 nm are deposited. The weight percentage of Ni_3S_2 nanoparticles loaded on MWCNTs ranges from 38 to 83%. For the MWCNT composite with 38 wt% Ni_3S_2 nanoparticles (Ni_3S_2(38%)/MWCNT-NC), the corresponding

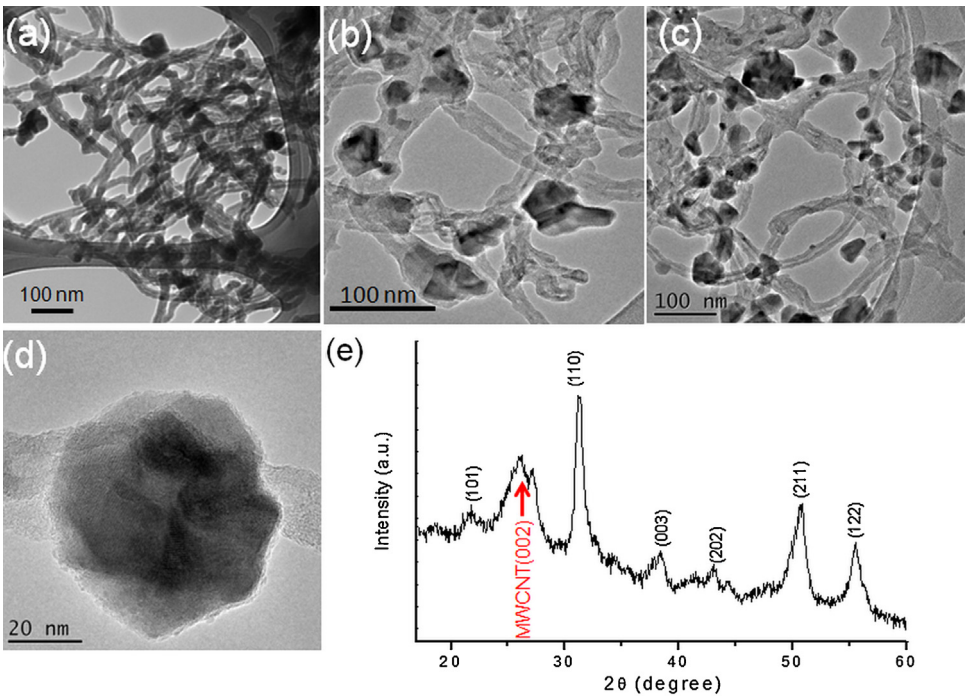

Fig. 1. Typical TEM images of (a) Ni_3S_2(38%)/MWCNT-NC, (b) Ni_3S_2(55%)/MWCNT-NC and (c) Ni_3S_2(83%)/MWCNT-NC. (d) High resolution TEM image and (e) XRD pattern of Ni_3S_2/MWCNT-NC.

TEM image (Fig. 1a) shows some nanoparticles are dispersed over the MWCNT surface. In Fig. 1b, the density of Ni_3S_2 nanoparticles on the MWCNT surface is enhanced when loading amount of Ni_3S_2 nanoparticles is increased from 38 to 55 wt%. For the MWCNT composite with 83 wt% Ni_3S_2 nanoparticles (Ni_3S_2(83%)/MWCNT-NC), it has the most dense population of Ni_3S_2 nanoparticles on the MWCNT surface (Fig. 1c) compared with other two composites. As shown in Fig. 1d, the high resolution TEM image of the composite shows a layer of amorphous carbon derived from glucose covers both MWCNT and nanoparticle surface and thus serves as a binder to assist the nanoparticles to grow along the longitudinal axis of MWCNTs [25]. The EDS analysis of the nanocomposite (Fig. S1) reveals the presence of C, O, Si, Ni and S elements and the atomic ratio of Ni to S is estimated to be 3.0:2.0. To further characterize the identity and structure of the composite sample, XRD measurement was carried out. As shown Fig. 1e, all the identified peaks except the (0 0 2) reflection of MWCNTs can be attributed to the Ni_3S_2 phase (JCPDS Card No. 30-0863).

3.2. Electrocatalytic activity of Ni_3S_2/MWCNT-NC toward HER

To test the catalytic activity of the Ni_3S_2/MWCNT-NC toward HER, the composite catalyst was drop-cast onto the Ag electrode and then the polarization measurement was carried out in a 1 M KOH solution. The catalytic activity of the silver electrode was first examined, which shows no obvious HER activity (Fig. S2). Fig. 2a shows the polarization curves of the different electrode materials. It is noted that pure MWCNTs or Ni_3S_2 powders exhibit the inferior HER activities to the composite catalysts. This result suggests that the electron transfer to the catalyst is significantly improved when Ni_3S_2 nanoparticles are directly deposited onto the conductive MWCNTs. Furthermore, it is also noted that the effect of the loading amount of Ni_3S_2 nanoparticles on MWCNT surface on HER activity is pronounced. When the Ni_3S_2 loading is 38 or 83 wt%, the relatively low catalytic activity is observed. Comparatively, the optimal Ni_3S_2 loading on MWCNTs is 55 wt%, which shows the highest catalytic activity among all the composite catalysts. For instance, the current densities of Ni_3S_2(55%)/MWCNT-NC are 1.2 and 13 mA/cm^2 at η = 400 and 500 mV, respectively. The difference in catalytic activity among the various nanocomposites may be attributed to the fact that the improvement of electron transfer in catalyst is highly correlated to the loading amount of MWCNTs in catalyst [26]. To further verify the aforementioned results, the EIS measurements on Ni_3S_2 (38–83%)/MWCNT-NC and Ni_3S_2 powder were performed. Fig. 2b shows Nyquist plots of the various HER catalysts. The semicircle in the high-frequency range of the Nyquist plot is attributed to the resistance capacitance network, consisting of the charge transfer resistance (R_{ct}) of H^+ reduction and the corresponding capacitance (C_{dl}) at the electrode–electrolyte interface [27,28]. Table 1 summarizes the R_{ct} values estimated by fitting the arc observed at high frequency with ZSimpWin software in terms of the equivalent circuit model (Fig. S3) [22]. It is noted that the R_{ct} value of Ni_3S_2 powder is the largest among all the catalysts; therefore, Ni_3S_2 powder shows the worst HER activity. In contrast, Ni_3S_2(55%)/MWCNT-NC has the low R_{ct} value of 244 Ω and thus shows superior HER activity to other composite catalysts, which is consistent with the result obtained from polarization measurements. The aforementioned EIS results verify that the incorporation of MWCNTs and their amount in the composite catalyst greatly influence electron transport and reaction kinetics during the HER [29].

In Fig. 3a, the current density of Ni_3S_2(55%)/MWCNT-NC gradually increases with the number of polarization scan. It seems that the HER activity of the composite catalyst is enhanced with the prolonged immersion in a KOH solution. To confirm the activation of the composite in a KOH solution, the electrode of Ni_3S_2(55%)/MWCNT-NC was immersed in a 30 wt% KOH solution for 12 h and then examined by polarization measurement. As shown in Fig. 3b, the KOH-treated Ni_3S_2(55%)/MWCNT-NC has a much larger current density than as-synthesized composite, which suggests that the former shows a better HER activity. Furthermore, the inset in Fig. 3b shows that the KOH-treated composite possess a smaller Tafel slope than as-synthesized composite. To further verify that the optimal Ni_3S_2 loading in composite catalyst is 55 wt%,

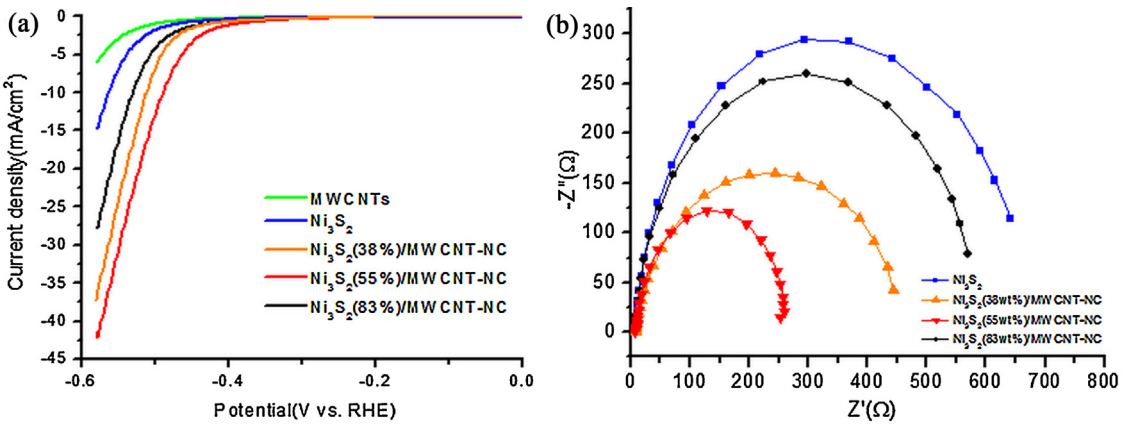

Fig. 2. (a) Polarization curves and (b) Nyquist plots of the various HER catalysts.

Table 1
EIS and kinetic parameters of MWCNT composites loaded with various amount of Ni_3S_2.

	R_{ct} (Ω)	Tafel slope (mV per decade)	Exchange current density (A cm^{-2})	$j_{\eta=580}$ (mA/cm^{-2})
Ni_3S_2	596	101	1.9×10^{-8}	14.6
Ni_3S_2(38%)/MWCNT-NC	360	157	2.0×10^{-6}	37.2
Ni_3S_2(55%)/MWCNT-NC	244	167	4.8×10^{-6}	41.5
Ni_3S_2(83%)/MWCNT-NC	537	183	4.6×10^{-6}	27.5
KOH-treated Ni_3S_2(55%)/MWCNT-NC	33	102	7.5×10^{-6}	107.3

the HER activities of the composites with the Ni_3S_2 loadings ranging from 38 to 83 wt% were examined after the KOH treatment. As shown in Fig. S4a, a series of the polarization measurements show that the HER activities of composite catalysts with various Ni_3S_2 loadings are significantly enhanced after the KOH treatment. For example, the current density of the activated Ni_3S_2(83%)/MWCNT-NC at $\eta = 580$ mV is approximately two times higher than that of as-synthesized one. Furthermore, the dependence of the HER activity of the composite catalyst on the loading amount of Ni_3S_2 nanoparticles is obviously observed. As shown in Fig. S4b, when the Ni_3S_2 loading amount is elevated from 38 to 55 wt%, the HER activity of Ni_3S_2/MWCNT composite increases with the Ni_3S_2 loading. However, the HER activity of Ni_3S_2/MWCNT composite begins to fall once the Ni_3S_2 loading on MWCNTs exceeds 55 wt%. The current densities of Ni_3S_2(55%)/MWCNT-NC at $\eta = 200$, 400 and 580 mV are much higher than those of other composite catalysts. As a result, Ni_3S_2(55%)/MWCNT-NC has the highest HER activity than other composite catalysts. This result suggests that the maximum

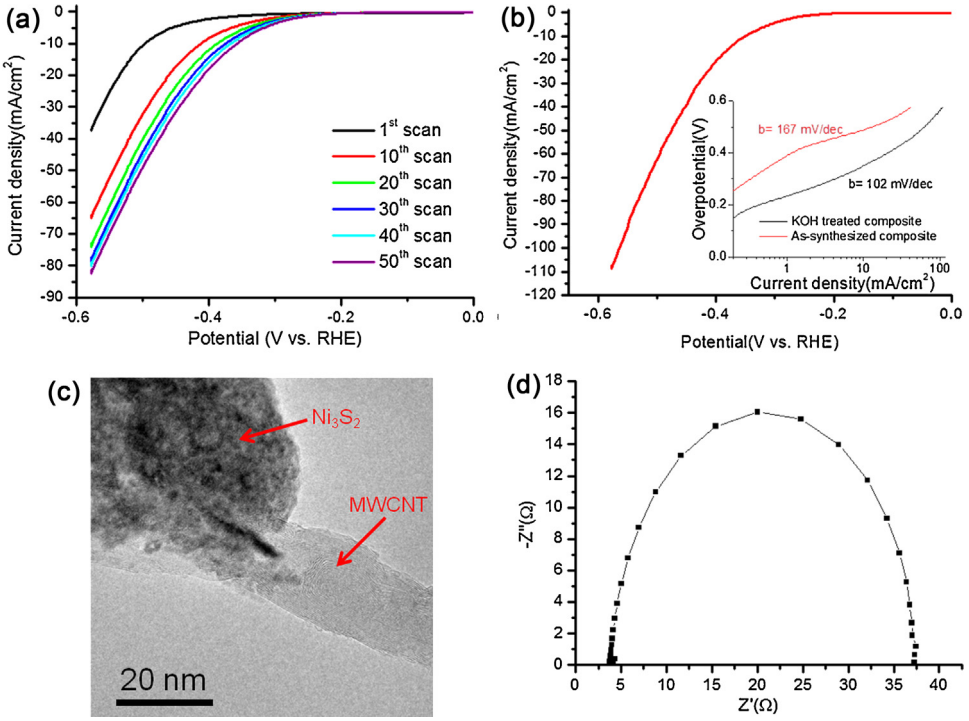

Fig. 3. (a) Current density of Ni_3S_2(55%)/MWCNT-NC as a function of the number of polarization scan. (b) Polarization curve, (c) TEM image and (d) Nyquist plot of the KOH-treated Ni_3S_2(55%)/MWCNT-NC. The inset in (b) shows Tafel plots of the Ni_3S_2(55%)/MWCNT-NC before and after base treatment.

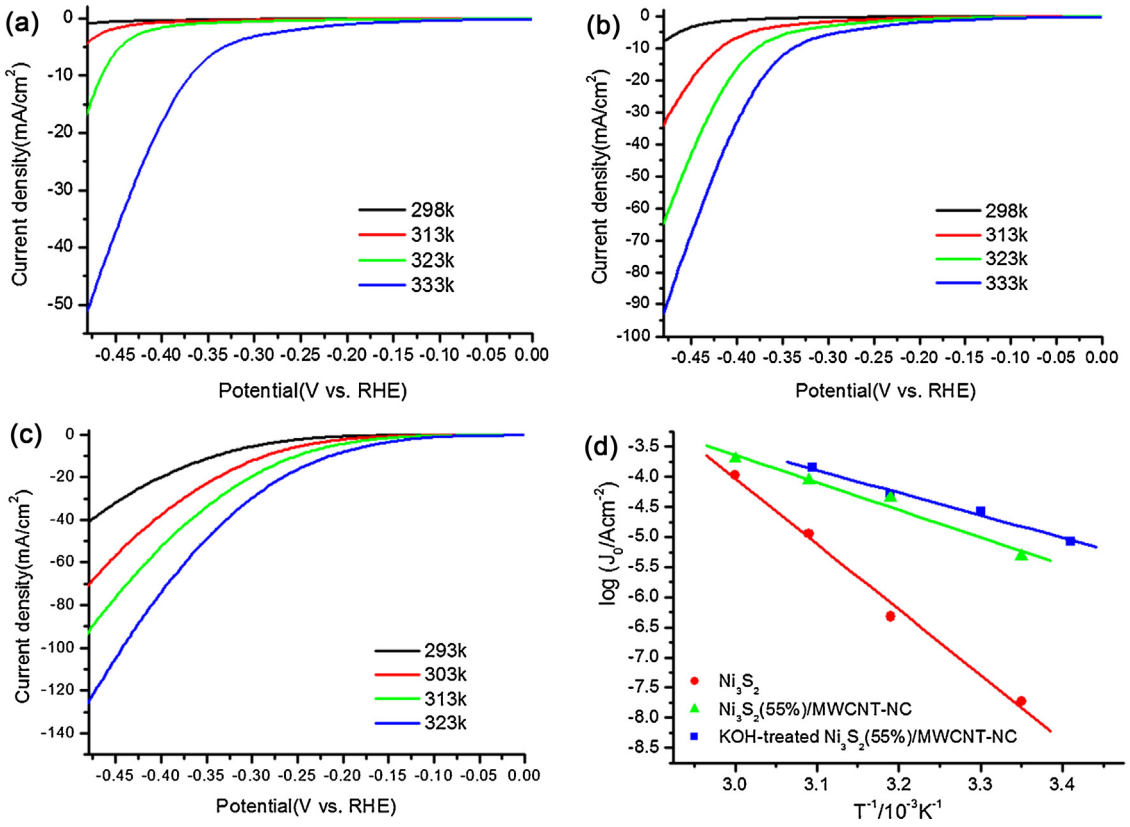

Fig. 4. Polarization curves of (a) Ni_3S_2 electrode (b) Ni_3S_2(55%)/MWCNT-NC and (c) KOH-treated Ni_3S_2(55%)/MWCNT-NC in 1.0 M KOH at different temperatures. (d) Arrhenius curves of three different electrodes.

HER activity of the composite catalyst can be achieved by tuning a weight ratio of MWCNT to Ni_3S_2, which is consistent with the previous studies of other composite catalysts for HER [22,26,29]. To understand the origin of the HER enhancement of the composite catalyst, the composite after base treatment was characterized by TEM and XRD. As shown in Fig. 3c, the surface of Ni_3S_2 nanoparticle in KOH-treated Ni_3S_2(55%)/MWCNT-NC is rougher than that in as-synthesized composite (Fig. 1d). This result suggests that base treatment induces the morphological change of the Ni_3S_2 nanoparticles, which leads to the increase in surface area of the catalysts. It is noted that the composition of the Ni_3S_2 nanoparticles deposited on MWCNT surface remains unchanged after the KOH treatment (Fig. S5). Furthermore, it is reasoned that the weight ratio of Ni_3S_2 nanoparticles to MWCNTs should be unchanged after the KOH treatment due to the fact that the HER activity of composite catalyst is strongly dependent on the loading amount of Ni_3S_2 on MWCNT surface (Fig S4). It is known that sodium hydroxide can serve as an efficient agent to remove the carbonaceous material on the surface of carbon nanotubes [30]. Therefore, it is assumed that the surface roughness of Ni_3S_2 nanoparticles may be attributed to the partial removal of carbonaceous material covered on Ni_3S_2 nanoparticles by KOH solution. As a result, more active sites in Ni_3S_2 nanoparticles could be exposed after the KOH treatment. However, the actual reasons for morphological change of the composite, requiring intense research efforts, are currently under investigation in our group. To further verify the aforementioned result, the EIS measurements on KOH-treated Ni_3S_2(55%)/MWCNT-NC was performed. It is observed from Fig. 3d that the R_{ct} value (33 Ω) of KOH-treated Ni_3S_2/MWCNT-NC is much smaller than that of as-synthesized composite, suggesting that the former has rapider electron-transfer kinetics at the electrode/electrolyte interface [29]. Furthermore, it is noteworthy that the C_{dl} value of KOH-treated Ni_3S_2(55%)/MWCNT-NC (0.31 mF) is about two times larger than that of untreated Ni_3S_2(55%)/MWCNT-NC (0.14 mF). The high C_{dl} value of the KOH-treated Ni_3S_2(55%)/MWCNT-NC reflects its large active surface area which can highly promote its HER activity [22,31].

Increasing the electrolytic temperature is an efficient way to reduce the voltage required for HER reaction. In this study, the effect of the electrolytic temperatures on the HER activities of the Ni_3S_2(55%)/MWCNT-NC and Ni_3S_2 electrodes is investigated. Fig. 4a–c shows the polarization curves of the three electrodes at different temperatures. For three different electrodes, their HER overpotentials decrease with increasing the electrolytic temperatures. For example, the overpotential of KOH-treated Ni_3S_2(55%)/MWCNT-NC at current density of 10 mA/cm^2 is decreased from 340 to 210 mV when the electrolytic temperature is elevated from 293 to 323 K. The kinetic parameters of three electrodes at various temperatures estimated from the Tafel plots (Fig. S6) are summarized in Table 2. It is evident from Table 2 that exchange current densities (J_0) of three electrodes are increased with the electrolytic temperature. Furthermore, the value of E_a for HER which is usually used to evaluate the intrinsic catalytic activity of the electrode can be estimated from Arrhenius curve of the electrode [32–34]. Based on the slopes of the regression lines shown in Fig. 4d, the E_a values of three different electrodes can be calculated. Compared with the Ni_3S_2 electrode, the electrode of Ni_3S_2(55%)/MWCNT-NC has a smaller E_a value and thus shows a higher HER activity. This result is supported by the fact that the R_{ct} value of Ni_3S_2(55%)/MWCNT-NC is lower than that of Ni_3S_2 electrode. The high HER activity of Ni_3S_2(55%)/MWCNT-NC may be attributed to the presence of a conductive MWCNT network in the catalyst. Furthermore, the E_a value of Ni_3S_2(55%)/MWCNT-NC is decreased from 87.4 to 71.8 kJ/mol after the composite electrode is subject to base treatment. For Ni_3S_2(55%)/MWCNT-NC electrode, the decrease in its E_a value means the enhancement of HER activity.

Table 2
Kinetic parameters of the Ni_3S_2 electrode, Ni_3S_2(55%)/MWCNT-NC and KOH-treated Ni_3S_2(55%)/MWCNT-NC.

Electrode	T (K)	Tafel slope (mV per decade)	Exchange current density (A cm^{-2})	E_a (kJ/mol)
Ni_3S_2	298	101	1.9×10^{-8}	208.1
	313	121	4.8×10^{-7}	
	323	188	1.1×10^{-5}	
	333	203	1.1×10^{-4}	
Ni_3S_2(55%)/MWCNT-NC	298	167	4.8×10^{-6}	87.4
	313	191	4.6×10^{-5}	
	323	194	8.7×10^{-5}	
	333	202	2.0×10^{-4}	
KOH-treated Ni_3S_2(55%)/MWCNT-NC	293	102	8.5×10^{-6}	71.8
	303	103	2.7×10^{-5}	
	313	102	5.2×10^{-5}	
	323	109	1.4×10^{-4}	

Such improvement may be attributed to the increase in the active surface area of Ni_3S_2(55%)/MWCNT-NC after base treatment.

In terms of E_a value, KOH-treated Ni_3S_2(55%)/MWCNT-NC shows a comparable catalytic activity to the electrodes constructed by NiFeZn alloy (62 kJ/mol) [32] or amorphous Ni–S alloy (72.8 kJ/mol) [33], and is even more active than phytic acid-coated titanium electrode (86 kJ/mol) [34]. Finally, the test of long-term stability of KOH-treated Ni_3S_2(55%)/MWCNT-NC was performed. As shown in Fig. 5, the current density of composite electrode shows no sign of degradation after the continuous 1000 cycling. Overall, KOH-treated Ni_3S_2(55%)/MWCNT-NC shows an excellent HER activity and the reasonable stability in the long-term operation.

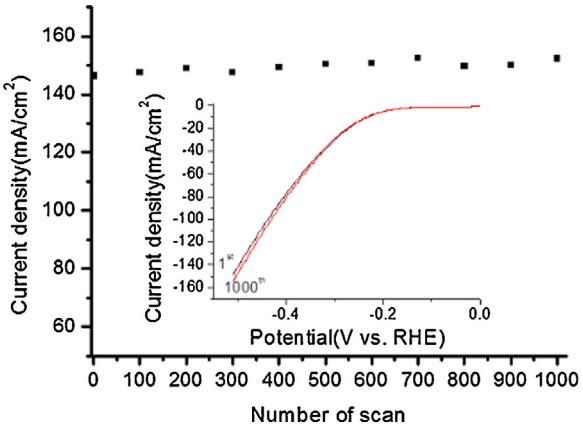

Fig. 5. The stability test for KOH-treated Ni_3S_2(55%)/MWCNT-NC in a 1 M KOH solution at the temperature of 323 K. The scan rate is 100 mV/s and scan region ranges from 0 V to −0.5 V vs. RHE.

3.3. Ni_3S_2/MWCNT-NC electrode for enzyme-free glucose detection

Recently, some transition metal sulfide nanoparticles including FeS, CuS and CdS have been demonstrated for their excellent

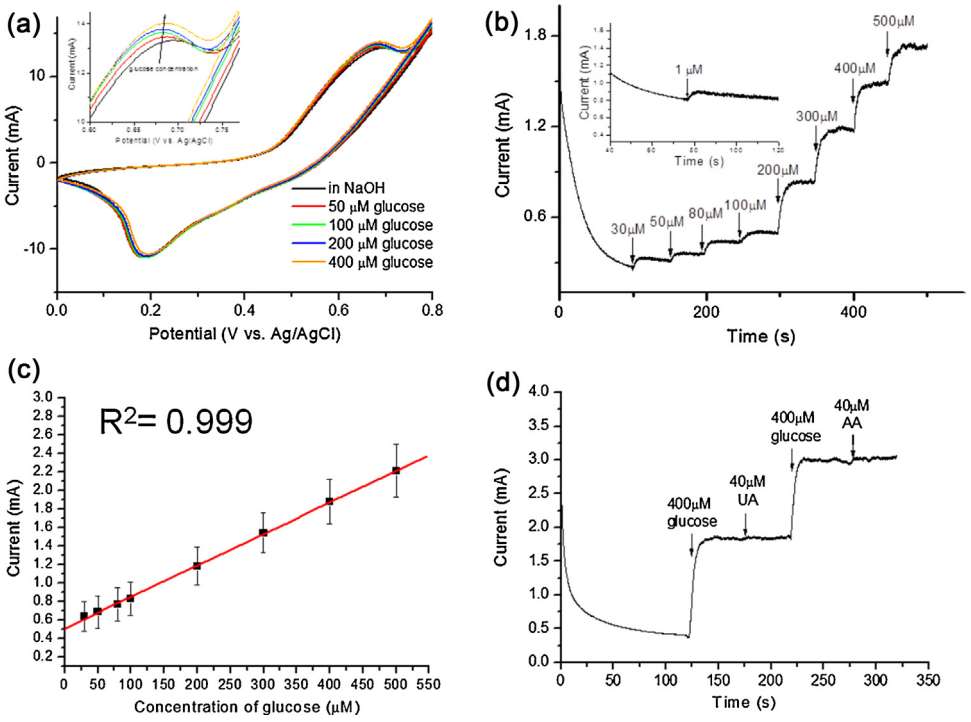

Fig. 6. (a) CV curves of the composite electrode recorded at a scan rate of 10 mV/s in 0.1 M NaOH solution containing the various concentrations of glucose. The inset in (a) shows the magnified plot in the potential window of 0.6–0.75 V. (b) Amperometric response of the composite electrode (holding at 0.54 V) to the glucose solutions with various concentrations. The inset in (b) shows the amperometric response to 1 μM glucose. (c) The plot of electrocatalytic current of composite electrode vs. the glucose concentration. Each data point in (c) represents the mean ± SEM of at least three measurements. (d) Amperometric response to the interfering biomolecules including UA and AA.

electrocatalytic activity toward glucose and hydrogen peroxide [35–38]. Inspired by the aforementioned studies, we attempted to explore the application of Ni_3S_2/MWCNT-NC as the enzyme-free glucose sensor. In Fig. 6a, the CV curve of Ni_3S_2/MWCNT-NC in a 0.1 M NaOH solution exhibits a pair of redox peaks in the potential range from 0 to 0.8 V. It is noteworthy that the anodic current is strongly influenced by the addition of glucose to NaOH solution. As shown in the inset of Fig. 6a, the anodic current increases with the concentration of glucose solution. The enhancement of anodic current may be attributed to the oxidation of glucose to glucolactone [39]. To identify the origin of the sensing of glucose, a separate experiment where bare MWCNTs served as a working electrode was performed. As shown in Fig. S7, the redox peaks of MWCNT electrode are shifted toward the positive potential compared to those of the composite electrode. More importantly, the MWCNT electrode shows a negligible response to the addition of 400 μM glucose solution. This result suggests that the Ni_3S_2 nanoparticles deposited on the MWCNT surface exhibit strong electrocatalytic activity toward glucose oxidation. Fig. 6b shows the amperometric response of the electrode of Ni_3S_2/MWCNT-NC upon the successive addition of a certain concentration of glucose into stirred 0.1 M NaOH. As shown in the inset of Fig. 6b, the detection limit can reach as low as 1 μM based on a signal-to-noise ratio of 3. Furthermore, the catalytic current shows a linear dependence on the concentration of glucose in the range from 30 to 500 μM and the sensitivity is as high as 3345 μA/mM (Fig. 6c). In order to evaluate the performance of the glucose sensor, a comparison of the electrode of Ni_3S_2/MWCNT-NC with other non-enzymatic glucose sensors constructed by the composite of nickel oxide (NiO) and CNs are carried out [39–43]. In terms of sensitivity, linear calibration range and limit of detection, the electrode of Ni_3S_2/MWCNT-NC is comparable with or even better than NiO/CN composite electrodes. To assess the selectivity of the biosensor based on Ni_3S_2/MWCNT-NC, two interfering biomolecules such as uric acid (UA) and ascorbic acid (AA) are examined. As shown in Fig. 6d, the biosensor exhibits a negligible response to UA and AA and maintains a good response to the subsequent glucose addition. Therefore, the current study demonstrates the application of Ni_3S_2/MWCNT-NC as a highly sensitive and selective biosensor for glucose.

4. Conclusions

The nanocomposite of Ni_3S_2 and MWCNTs with the high catalytic activities toward HER and glucose oxidation can be synthesized by glucose-assisted hydrothermal method. The TEM images of the nanocomposites show the conductive MWCNTs can serve as the backbone where the Ni_3S_2 nanoparticles with the diameters ranging from 10 to 80 nm are deposited. The HER activity and kinetics of Ni_3S_2/MWCNT-NC have been studied by the polarization and EIS measurements. It is observed that the catalytic activity of Ni_3S_2/MWCNT-NC is increased with decreasing the Ni_3S_2 loading on MWCNTs and the optimal loading amount of Ni_3S_2 on MWCNTs is 55 wt%. Furthermore, the HER activity of Ni_3S_2(55%)/MWCNT-NC can be further improved by treating the composite electrode in a 30 wt% KOH solution. Based on the TEM images of KOH-treated composite, the base treatment induces that the surface of Ni_3S_2 nanoparticles on MWCNTs becomes rough. As evidenced by the increase in the C_{dl} value of composite electrode, the active surface area of composite electrode is enlarged after base treatment. Therefore, the HER activity of composite electrode after base treatment is enhanced. Moreover, the catalytic activities of the Ni_3S_2 and Ni_3S_2/MWCNT-NC electrodes toward the HER have been investigated as a function of temperature. The E_a values of Ni_3S_2 and Ni_3S_2(55%)/MWCNT-NC electrodes are 208.1 and 87.4 kJ/mol, respectively. In sharp contrast, the lowest E_a value (71.8 kJ/mol) has been obtained for the KOH-treated Ni_3S_2(55%)/MWCNT-NC and thus this electrode shows the best intrinsic catalytic activity among all the electrodes. The high HER activity of KOH-treated Ni_3S_2(55%)/MWCNT-NC may be attributed to the synergistic effect from the conductive network of MWCNTs and the large active surface area of Ni_3S_2 nanoparticles. Furthermore, it is found that KOH-treated Ni_3S_2(55%)/MWCNT-NC shows no sign of degradation after the continuous 1000 cycling in a 1 M KOH solution at the temperature of 323 K.

On the other hand, an attempt has been carried out to use Ni_3S_2/MWCNT-NC electrode as the glucose sensor. It is found that the Ni_3S_2 nanoparticles deposited on MWCNTs exhibit high electrocatalytic activity toward glucose oxidation and are insensitive to two interfering biomolecules such as UA and AA. The composite electrode exhibits that its catalytic current is linearly dependent on the concentration of glucose in the range from 30 to 500 μM and its sensitivity is as high as 3345 μA/mM. The present work suggests that the Ni_3S_2/MWCNT-NC not only serves as an inexpensive, highly active and stable electrode material for alkaline water electrolysis, but also shows a great potential application as a highly sensitive and selective biosensor for glucose.

Acknowledgements

This research was supported by National Science Council Taiwan (NSC 102-2113-M-029-001-MY2). This research was also supported by Tunghai Green Energy Development and Management Institute (TGEI).

Appendix A. Supplementary data

Supplementary material related to this article can be found, in the online version, at http://dx.doi.org/10.1016/j.apcatb.2014.02.017.

References

[1] J.A. Turner, Science 305 (2004) 972.
[2] J. Nowotny, C.C. Sorrell, L.R. Sheppard, T. Bak, Int. J. Hydrogen Energy 30 (2005) 521.
[3] M.A. Rosen, D.S. Scott, Int. J. Hydrogen Energy 23 (1998) 653.
[4] D. Trommer, F. Noembrini, A. Fasciana, D. Rodriguez, A. Morales, M. Romero, A. Steinfeld, Int. J. Hydrogen Energy 30 (2005) 605.
[5] P.D. Tran, L.H. Wong, J. Barber, J.S.C. Loo, Energy Environ. Sci. 5 (2012) 5902.
[6] X.J. Lv, W.F. Fu, H.X. Chang, H. Zhang, J.S. Cheng, G.J. Zhang, Y. Song, C.Y. Hu, J.H. Li, J. Mater. Chem. 22 (2012) 1539.
[7] M.G. Walter, E.L. Warren, J.R. McKone, S.W. Boettcher, Q.X. Mi, E.A. Santori, N.S. Lewis, Chem. Rev. 110 (2010) 6446.
[8] M.B.I. Janjua, R.L. Le Roy, Int. J. Hydrogen Energy 10 (1985) 11.
[9] J.Y. Huot, L. Brossard, Int. J. Hydrogen Energy 12 (1987) 821.
[10] H.E.G. Rommal, P.J. Moran, J. Electrochem. Soc. 132 (1985) 325.
[11] D.M. Soares, O. Teschke, I. Torriani, J. Electrochem. Soc. 139 (1992) 98.
[12] D.E. Brown, M.N. Mahmood, M.C.M. Man, A.K. Turner, Electrochim. Acta 29 (1984) 1551.
[13] D.L. Chonglun Fan, Piron, P. Abderrahman Sleb, Paradis, J. Electrochem. Soc. 141 (1994) 382.
[14] H.B. Suffredini, J.L. Cerne, F.C. Crnkovic, S.A.S. Machado, L.A. Avaca, Int. J. Hydrogen Energy 25 (2000) 415.
[15] I. Herraiz-Cardona, E. Ortega, V. Pérez-Herranz, Electrochim. Acta 56 (2011) 1308.
[16] Z. Zheng, N. Li, C.Q. Wang, D.Y. Li, F.Y. Meng, Y.M. Zhu, Q. Li, G. Wu, J. Power Sources 230 (2013) 10.
[17] H. He, H. Liu, F. Liu, K. Zhou, Surf. Coat. Technol. 201 (2006) 958.
[18] Q. Han, K. Liu, J. Chen, X. Wei, Int. J. Hydrogen Energy 28 (2003) 1207.
[19] Th. Borucinsky, S. Rausch, H. Wendt, J. Appl. Electrochem. 27 (1997) 762.
[20] I. Paseka, Electrochim. Acta 38 (1993) 2449.
[21] Y. Li, H. Wang, L. Xie, Y. Liang, G. Hong, H. Dai, J. Am. Chem. Soc. 133 (2011) 7296.
[22] T.W. Lin, C.J. Liu, J.Y. Lin, Appl. Catal. B: Environ. 134–135 (2013) 75.
[23] P. Paunovic, O. Popovski, A. Dimitrov, D. Slavkov, E. Lefterova, S. Hadzi Jordanov, Electrochim. Acta 52 (2007) 4640.
[24] P. Paunovic, I. Radev, A.T. Dimitrov, O. Popovski, E. Lefterova, E. Slavcheva, S.H. Jordanov, Int. J. Hydrogen Energy 34 (2009) 2866.
[25] S.J. Ding, J.S. Chen, X.W. Lou, Chem. Eur. J. 17 (2011) 13142.

[26] H. Vrubel, D. Merki, X. Hu, Energy Environ. Sci. 5 (2012) 6136.
[27] J. Kubisztal, A. Budniok, A. Lasia, Int. J. Hydrogen Energy 32 (2007) 1211.
[28] I. Dannee, S. Noori, Int. J. Hydrogen Energy 36 (2011) 12102.
[29] Y. Yan, B. Xia, X. Qi, H. Wang, R. Xu, J.Y. Wang, H. Zhang, X. Wang, Chem. Commun. 49 (2013) 4884.
[30] C.G. Salzmann, S.A. Llewellyn, G. Tobias, M.A.H. Ward, Y. Huh, M.L.H. Green, Adv. Mater. 19 (2007) 883.
[31] D. Merki, H. Vrubel, L. Rovelli, S. ˙Fierro, X. Hu, Chem. Sci. 3 (2012) 2515.
[32] M.J. Giz, S.C. Bento, E.R. Gonzalez, Int. J. Hydrogen Energy 25 (2000) 621.
[33] Z. Shan, Y. Liu, Z. Chen, G. Warrender, J. Tian, Int. J. Hydrogen Energy 33 (2008) 28.
[34] B. Liu, J.B. He, Y.J. Chen, Y. Wang, N. Deng, Int. J. Hydrogen Energy 38 (2013) 3130.
[35] J. Liu, D. Xue, J. Mater. Chem. 21 (2011) 223.
[36] S.K. Maji, A.K. Dutta, P. Biswas, D.N. Srivastava, P. Paul, A. Mondal, B. Adhikary, Appl. Catal. A: Gen. 419–420 (2012) 170.
[37] S.K. Maji, A.K. Dutta, D.N. Srivastava, P. Paul, A. Mondal, B. Adhikary, J. Mol. Catal. A: Chem. 358 (2012) 1.
[38] A.K. Dutta, S.K. Maji, A. Mondal, B. Karmakar, P. Biswas, B. Adhikary, Sens. Actuators B 173 (2012) 724.
[39] Y. Zhang, F. Xu, Y. Sun, Y. Shi, Z. Wen, Z. Li, J. Mater. Chem. 21 (2011) 16949.
[40] Y. Zhang, Y. Wang, J. Jia, J. Wang, Sens. Actuators B 171–172 (2012) 580.
[41] M. Shamsipur, M. Najafi, M.R. Milani Hosseini, Bioelectrochemistry 77 (2010) 120.
[42] W.D. Zhang, J. Chen, L.C. Jiang, Y.X. Yu, J.Q. Zhang, Microchim. Acta 168 (2010) 259.
[43] W. Lv, F.M. Jin, Q. Guo, Q.H. Yang, F. Kang, Electrochim. Acta 73 (2012) 129.